EurJIC
European Journal of Inorganic Chemistry

Minireview
doi.org/10.1002/ejic.202000834

MOFs for Heat Transformation

Metal-Organic Frameworks as Sorption Materials for Heat Transformation Processes

Dominik Moritz Steinert,[a] Sebastian-Johannes Ernst,[b] Stefan K. Henninger,[b] and Christoph Janiak*[a]

Dedicated to Prof. Dr. Erwin Riedel on the occasion of his 90th birthday.

Abstract: Cyclic physical adsorption and desorption processes on porous materials can be used for the conversion of heat in heat transformation processes, which is the working principle in adsorption heat pumps (AHPs). Environmentally benign water with its high enthalpy of evaporation is the working fluid of choice in AHPs. Metal-organic frameworks, MOFs can adsorb large amounts of water or methanol, up to their own weight. MOFs could be alternative materials to silica gels, zeolites, or aluminum phosphates for low-temperature heat transformations in AHPs.

Introduction

Metal-organic frameworks (MOFs) are potentially porous coordination networks composed of metal nodes and organic linkers that self-assemble into an extended (crystalline) two- or three-dimensional network (Figure 1).[1–3] Their high internal surface area and a large pore volume, adjustable three-dimensional structure, and tunable inner and outer microenvironment let one envision MOFs for a myriad of applications,[4–7] most prominently in gas storage and separation,[8,9] as porous fillers in mixed-matrix membranes,[10–14] catalysis,[15] drug delivery,[16,17] enzyme immobilization, etc.[18] as filler in mixed-matrix membranes etc.

Since their discovery in the early 1990s, MOFs have proven to be more and more suitable for a task- and compound-specific adsorption of gases and vapors.[4–7] Compared to other sorption materials such as activated carbons, silica gels, or zeolites, the sorption properties of MOFs can be better tailored via the organic ligands. Due to the chemical robustness of MOFs, the ligands can be modified by organic-chemical reactions (substitutions, additions) even after MOF network synthesis. For this purpose, the term "post-synthetic modification" has been coined for MOFs.[19] In a simplified picture, zeolites and silica gels have only SiO_4 and AlO_4 building blocks which are connected via corners into networks. A modification of the assembly of these building blocks is only possible within relatively narrow limits when compared to MOFs. For the latter, the essentially infinite variety of organic chemistry is available for the modification of MOF ligands. MOFs are record holders for the size of the internal surface area. Specific inner surface areas of MOFs typically range from 1000–4000 m^2/g, but values above 6000 m^2/g have also been reported (MIL-210 or NU-100).[20] In contrast, the specific inner surface areas of zeolites and silica gels are at 1000 m^2/g and below. The pore openings or channel diameters in MOFs range from 0.3 to 3.4 nm, with specific pore volumes up to 1.5–2 cm^3/g. An advantage of MOFs over amorphous sorption materials such as activated carbon or silica gel is their perfectly identical pore size over the entire network structure. In contrast, activated carbons and silica gels are

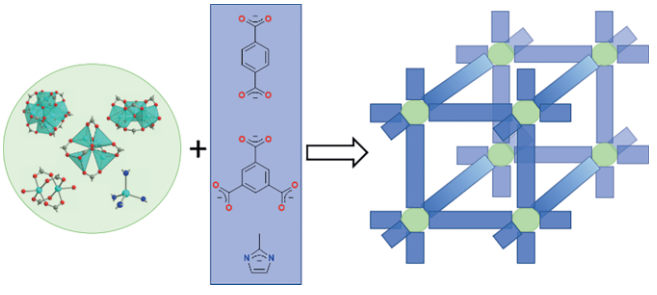

Figure 1. Construction principle of MOFs from metal clusters or metal atoms (examples shown with their attached donor atoms from ligands with carboxylate, $-CO_2$ or azolate, -N groups) and organic ligands (linkers) into a three-dimensional porous framework.

[a] D. M. Steinert, C. Janiak
Institut für Anorganische Chemie und Strukturchemie,
Heinrich-Heine-Universität,
40204 Düsseldorf, Germany
E-mail: janiak@hhu.de
https://www.ac1.hhu.de
[b] Dr. S.-J. Ernst, Dr. S. K. Henninger
Dept. Thermally Active Materials and Solar Cooling, Fraunhofer Institute for Solar Energy Systems ISE,
Heidenhofstr. 2, 79110 Freiburg, Germany
https://www.ise.fraunhofer.de
ORCID(s) from the author(s) for this article is/are available on the WWW under https://doi.org/10.1002/ejic.202000834.

Part of the German Chemical Society ADUC Prizewinner Collection

amorphous materials, so their microstructure is not precisely known.

In the last few years, water sorption has become an increasingly important research field.[21,22] This also includes the possible use of porous materials to adsorb and desorb water vapor under atmospheric conditions without external power sources as a promising methodology for the capture and release of water in arid or desert regions of the world. The potential of metal-organic frameworks as water harvesting materials for freshwater production in dry regions with medium or high humidity conditions during the night appears to have first been tested by Kim et al.[23] and Trapani et al. in 2016,[24] The possible generation of drinking water through the adsorption of moisture from the air was then followed-up by Yaghi and co-workers in 2017. The energy-efficient adsorption of atmospheric water and its separation for subsequent use still represents a technical and economic challenge.[25–29]

One obstacle on the way to broader applications of MOFs has long been their insufficient hydrothermal stability (see below).[30] However, in the meantime MOFs are known to be stable against prolonged contact with water, and not only because of their high hydrophobicity (as with ZIF-8). This has opened up the potential application of cyclic water sorption with water-stable MOFs in adsorption heat pumps (AHPs), including adsorption chillers.[31] Physical adsorption and desorption processes on inner surfaces of highly porous materials, can be used to convert heat in heat transformation processes.[32] Adsorption is a process of adhesion of atoms, molecules, or ions of a gas or liquid at the surface of a solid or liquid. Most research focuses on adsorption on the solid surface and physisorption, i.e. the process in which the adsorbed species do not form chemical bonds with the surface but only bind through physical forces (dispersion, electrostatic, etc.).

A simple setup illustrates the working cycle (Figure 2) in which cold is generated, which can be used for cooling processes, from the evaporation of water which is driven by adsorption into the activated porous sorption material.

Figure 3 depicts the underlying principle of closed cycling adsorption heat transformation systems. The heart of such systems is the working pair consisting of an adsorbent and a working fluid. During the first stage of this two-stage-process, the active (dry, porous) adsorbent physisorbs the working fluid that is evaporated by taking up heat (Q_{in}) and thereby generating useful cold. The released heat of adsorption in the adsorbent is led away or used as heat ($Q_{out,1}$). During the desorption stage, heat has to be applied to the filled (wet) adsorbent (Q_{drive}) in order to induce the desorption of the working fluid. The working fluid is condensed by leading away or using the heat of condensation ($Q_{out,2}$) on a medium temperature level. $Q_{out,1}$ and $Q_{out,2}$ can be applied as usable heats for heating purposes.

Dominik Moritz Steinert *studied Business Chemistry and Chemistry at the Heinrich-Heine-University Düsseldorf and received his Master degree in 2017. Since then he works as a PhD student at the Heinrich-Heine University within the section of Bioinorganic chemistry under the supervision of Prof. Christoph Janiak. His research focuses on the synthesis, characterization and development of metal organic frameworks (e.g. MOFs).*

Sebastian-Johannes Ernst *studied chemical engineering at the Karlsruhe Institute of Technology and received his Diploma degree in 2014. Since then, he works at Fraunhofer Institute for Solar Energy Systems within the Division Thermal Systems and Building Technologies and did his doctorate on the topic Development and Characterization of Advanced Materials for Heat Transformation Applications under supervision of Prof. Bart/TU Kaiserslautern. Since 2019 he is head of the group Service life and material analysis.*

Stefan Kai Henninger *studied physics at the University of Freiburg and received his Diploma degree in 2002. He did his PhD at the Freiburg Material Research Center (FMF) on the topic of new adsorbents for heat storage and transformation using Monte Carlo simulations. Since 2008, he worked at the Fraunhofer ISE on materials development and characterization being head of a research group until 2018. After being responsible for the IP management and strategy of a large project he switched his position to the department heating and cooling technologies as deputy head taking care of developments with focus on high temperature heat pumps for industrial applications.*

Christoph Janiak *is full professor at the Heinrich-Heine-University Düsseldorf since 2010, with research interests in porous materials (e.g. MOFs), mixed-matrix membranes, metal nanoparticles, ionic liquids and catalysis. Currently, he is a guest professor at the Hoffmann Institute of Advanced Materials at Shenzhen Polytechnic in China. He has (co-)authored about 530 research papers.*

Minireview
doi.org/10.1002/ejic.202000834

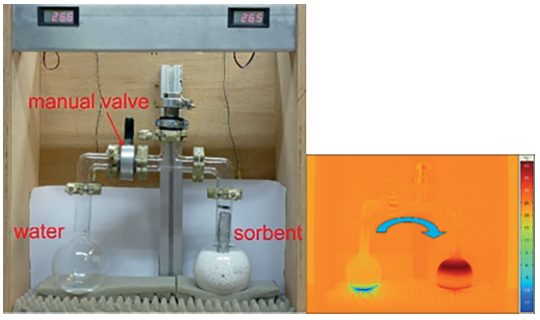

Figure 2. A simple experimental setup illustrates how the evaporation of water generates useful cold. After opening the manual valve, the water evaporates from the left-hand flask into the right-hand flask, driven by the adsorption into an empty, porous sorption material. Right: infrared image taken a few minutes after opening the manual valve. In the water flask the temperature drops to approx. –5 °C with the formation of ice; in the sorption material it rises to approx. 40 °C.[33,34] Reproduced from ref.[34]

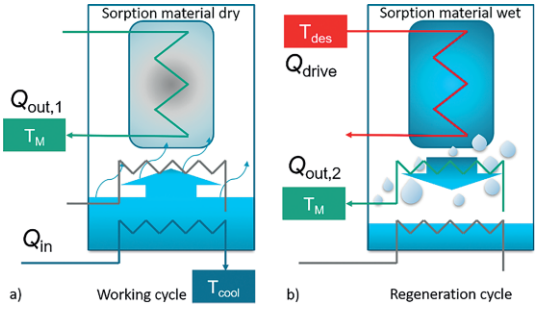

Figure 3. Schematic working principle of thermally-driven adsorption heat transformation. (a) In the working cycle, a working fluid (favorably water due to its high evaporation enthalpy and nontoxicity) is evaporated at a low-temperature level T_{cool} consuming the heat of evaporation Q_{in} which translates into useful cold. During adsorption into a porous material, heat of adsorption $Q_{out,1}$ is released at a medium temperature level T_M. (b) In the regeneration cycle, driving heat Q_{des} for desorption is applied at a high-temperature level T_{des}, to regenerate the adsorbent. The released working fluid is collected in a condenser and releases condensation heat $Q_{out,2}$ at the medium temperature level T_M. The device can be used as a chiller or a heat pump.

By reversing the adsorption and regeneration in few-minute intervals, a heat pump, including an air conditioning system can be set up. In the heating mode, the heat of adsorption ($Q_{out,1}$) and heat of condensation ($Q_{out,2}$) are utilized and Q_{in} presents the additional energy gain from the environment to Q_{drive} (ideally $Q_{out,1} + Q_{out,2} = Q_{drive} + Q_{in}$), determining the coefficient of performance for heating (COP_{HP}) (see below).

In the cooling mode cold is generated essentially from heating and adsorption heat transformation (AHT) can therefore operate much more energy-efficiently than conventional air conditioning systems operated with compressors (using electrical energy), if there is the chance to use waste heat which is otherwise lost.[35] For both modes, driving heat (Q_{drive}) can be supplied by often readily available waste heat (below 100 °C) from industrial processes, solar heat, or direct heat from a gas burner.[36,37]

So far, the inorganic materials silica gels and zeolites are already used in commercial adsorption coolers and adsorption heat pumps. At low humidity, zeolites adsorb water well with up to 0.26 g of water per gram zeolite (0.26 g/g) (Figure 4), but also require a high temperature of over 200 °C for regeneration.[38,39] Silica gels bind water less well than zeolites and require only about 100 °C for regeneration (see also below). However, silica gels have only a low water adsorption capacity in the relevant vapor pressure range of 0.13 g/g (Figure 4).[40]

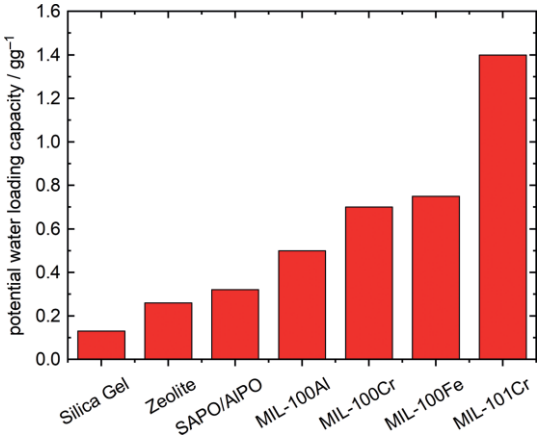

Figure 4. Comparison of typical water adsorption capacities of classical porous materials and MOFs of the MIL type,[68] for the possible use in adsorption driven heat pumps.[35] The loading capacity (in g of water/g of dry sorbent material) is the uptake or loading lift within an adsorption-desorption cycle. The water stability of some of the MIL networks was confirmed over a large number of adsorption and desorption cycles (MIL-100Al and MIL-100Fe,[67] MIL-100Cr,[66] MIL-101Cr[34]).

A sorption material for thermal adsorption chillers and adsorption heat pumps should have a high water adsorption capacity at low to medium relative humidity (5–35 %, that is 0.05 < p/p_0 < 0.35), release the water vapor below 80 °C and have a water uptake during each cycle of at least 0.3 g/g.[35,41] This value is two to three times higher than the mass-based g/g working capacity of silica gel within the stated boundaries.

A broad variety of different adsorbent-adsorbate working pairs is already investigated for sorption heat transformation.[37,42] Each one of these classes has its own distinct field of application, e.g. activated carbon-methanol for cooling, SAPO-34-water for heating, silica gel for certain cooling applications, zeolite 13X for heat storage, not to mention the vast variety of salt-based adsorbents and composites for any of these applications. Activated carbons are rather low-cost and hydrophobic materials and have high adsorption capacities for alcohol and ammonia.[43,44] Silica gel is one of the most used adsorbents in commercially available AHTs due to its low cost and stability, despite its less favorable linear water uptake curve instead of the S-shaped isotherm and low water uptake of 0.03 to 0.1 g/g.[45,46] The recently developed AHT technique "Heat from Cold" (HeCol) uses LiCl-silica gel/methanol as working pair.[47,48] LiBr-silica and $CaCl_2$-silica[49] appear to be superior composite adsorbents with the working fluid water for air conditioning and heat pumping. For refrigeration, where water freezes and cannot be used as adsorbate, LiBr-silica with methanol and ethanol was found as promising working pair.[50] One of the biggest disadvantages of standard zeolites for AHT is their quite high hydrophilicity, which necessitates desorption temperatures up to 120 °C.[51] Modified zeolites such as Mitsubishi's adsorbent

AQSOA®-FAM-Z02,[52–54] and the SAPO-34 zeolite[55] with water as adsorbate were similar in performance to the above-noted LiBr-silica and $CaCl_2$-silica.[50] Since the focus here is set to the use of MOFs, the reader is referred to a variety of publications for further reviewing and comparing different classes of adsorbents and adsorbent-adsorbate working pairs.[51,56–60]

Further, water is the natural choice as working fluid due to its non-toxicity and its high heat of evaporation (2258 kJ/kg). However, other working fluids even though inferior in the heat of evaporation come with advantages like higher pressure levels, less problems with hydrothermal stability (for the adsorbate), and a freezing point below 0 °C (to allow for refrigeration applications). These other working fluids are methanol (1100 kJ/kg), ethanol (838 kJ/kg), ammonia (1368 kJ/kg), and even difluoromethane (45 kJ/kg). The latter two have already been proposed and tested, e.g. with the working pair activated carbon/ammonia[32,61,62] and activated carbon/difluoromethane.[63] However, to the best of our knowledge ammonia and difluoromethane have not been tested with metal-organic frameworks with respect to their use in heat transformation. Regarding methanol, it has to be stated, that methanol itself showed instabilities (e.g. ether formation) at driving temperatures above 120 °C whereas there have been no such observations for ammonia.[51,64]

The group of late Prof. Gérard Férey from the Institute Lavoisier at the University of Versailles has produced highly porous, water-stable MOF materials called MILs (MIL = Materials of Institute Lavoisier).[65] MIL materials can adsorb significantly more water than zeolites (Figure 4).[33,35,66,67,68] The zeolite-like but inorganic-organic hybrid chromium terephthalate MOF MIL-101Cr can adsorb more than its own weight of water (Figure 4).[33–35,68] At the same time, the highly porous material MIL-101Cr is stable against water and heat for a long time. MIL-101Cr is among the MOF record holders for water uptake which however takes place at a slightly too high relative pressure of 0.4.[34]

How it Started

The development of cyclic water sorption in MOFs for heat transformation in the Janiak group started with the contact to Dr. Henninger in 2009 to employ the potential of MOFs with their high porosity as sorption material in heating and cooling applications. In the Janiak group, the doctoral student Hesham A. Habib had synthesized the MOF 3D-{[$Ni_3(\mu_3\text{-btc})_2(\mu_4\text{-btre})_2(\mu\text{-}H_2O)_2$]•ca. $22H_2O$} (Figure 5) in water as solvent. This MOF contained about 30 wt.-% of crystal water with about 22 disordered water molecules where the oxygen atoms with partially occupied position could be refined in the X-ray structure.[69] At the same time this MOF could be expected to be at least somewhat water stable, because it originated from this medium. When the cycling water sorption properties of this MOF were published,[70] the MOF was denoted as ISE-1 (ISE = [Fraunhofer] Institute for Solar Energy Systems). Using the MOF ISE-1, the possibility of using MOFs for cycling water sorption for heat transformation was experimentally demonstrated for the first time,[70] after a suggestion for MOFs for adsorptive heat pumping and storage had been put forward by Aristov.[71] Subsequently, Henninger and Janiak as well as other groups examined many aspects of this area. The main focus was on the hydrothermal stability of the MOFs in combination with uptake capacity, humidity region, and synthesis from inexpensive starting materials. Furthermore, shaping of the microcrystalline MOF powder became a focus that is extremely important for almost any industrial application.

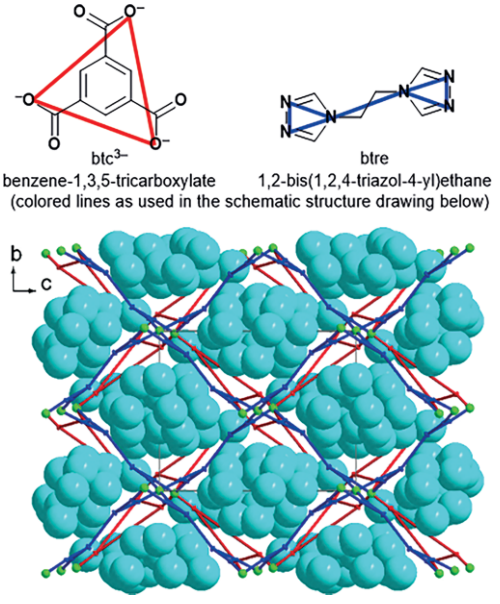

Figure 5. Schematic drawing of the 3D framework 3D-{[$Ni_3(\mu_3\text{-btc})_2(\mu_4\text{-btre})_2(\mu\text{-}H_2O)_2$]•ca. $22H_2O$} (btc ligand in red, btre ligand in dark blue, nickel atoms in green) with the oxygen atoms (light blue) of the water of crystallization in space-filling mode.[69,70] Reproduced from ref.[70] © (2009), with permission of the American Chemical Society.

Theory of Water Adsorption

The physisorption of water in porous materials can be described in two different parts, at first the attachment of layers or clusters of water molecules to surfaces or in pores until surface saturation. Subsequently, the continuous pore filling takes place, which occurs as capillary condensation in the case of small pore sizes.[72]

The capillary condensation depends on the so-called critical pore diameter (D_c), which in turn is temperature-dependent.[89] The variables included in the calculation are the van der Waals diameter of the adsorptive (σ), the measuring temperature (T), and the critical temperature of the adsorptive (T_c).[89]

$$D_c = \frac{4\sigma T_C}{(T_C - T)}$$

For water, D_c at 298 K is approximately 20 Å (2 nm). Porous materials are classified according to their pore size. According to IUPAC, microporous materials have pore sizes up to 2 nm, mesoporous ones between 2 to 50 nm, and macroporous ones have a pore diameter above 50 nm.[73] Up to the value of 2 nm the pore filling occurs continuously. At larger pore diameters the pore condensation leads to a hysteresis in the desorption isotherm.[72]

An S-shape of the sorption isotherm (IUPAC classification Type V)[74] is desirable which enables a large loading lift within a narrow relative pressure range and with the large uptake step, that is the steep rise and inflection point in the relative pressure range of $p/p_0 \approx 0.1–0.3$ for an effective usable adsorptive uptake.[75] The inflection point of the water sorption isotherms describes the relative hydrophilicity of the adsorbent. At this point, half of the maximum intake has been reached. The hydrophilicity of porous materials is a measure of the material's affinity for water, in a multi-component mixture. Hydrophilic linkers as well as small pore sizes move the inflection point to lower partial pressures.[89,76] For the uptake capacity, it is, however not the hydrophilicity, but the pore volume that is decisive.[89] The optimum inflection point and uptake pressure range should be tunable as they depend on the desired working conditions which can vary. Suitable for AHP applications are, in particular, those porous materials which have a high water uptake (adsorption) in a narrow partial pressure range and which show little to no hysteresis.[77,89] A hysteresis will reduce the usable part of the loading and lead to loss of sensible heat.[78,79] The partial pressure at which water adsorption takes place can be adjusted by pore size and hydrophilicity. These requirements make MOFs the most promising materials for further development of adsorbents for AHPs because of the easy fine-tuning of their hydrophilicity (see below). Figure 4 has already shown the advantage of MOFs in terms of water adsorption capacity.

The water sorption isotherm provides insight into the uptake mechanism and hydrophilicity/hydrophobicity of the material. Figure 6 shows five isothermal water adsorption profiles of adsorbents which differ in their hydrophilicity and porosity. A highly hydrophilic material, such as a zeolite but also a hydrophilic MOFs, such as HHU-1[80] with uniform micropores will have a steep uptake at very low p/p_0 due to strong adsorbent-adsorptive interactions in the narrow micropores from which a micropore filling at very low p/p_0 results (curve a in Figure 6). With lower hydrophilicity but still uniform microporosity, as in the MOFs NH_2-MIL-125,[81] aluminum fumarate (Alfum)[82] or CAU-10-H[78,83] the isotherm changes to an S-form with the uptake in the relative pressure range up to $p/p_0 \approx 0.3$ (curve b in 6).[84] If the material becomes more hydrophobic and may also include mesopores beside micropores, as MIL-101Cr[34] the steep S-rise shifts to higher p/p_0 (curve c in Figure 6) and may also become more gradual.[84] The isotherm curve d in Figure 6 is obtained with highly hydrophobic materials, such as activated carbons[85,86] or covalent triazine frameworks (CTFs).[87,88] There, the pores are only filled at high partial pressures. Silica gels lie with their hydrophilicity and amorphous micro-mesopore structure between these examples and show continuous water adsorption.[89]

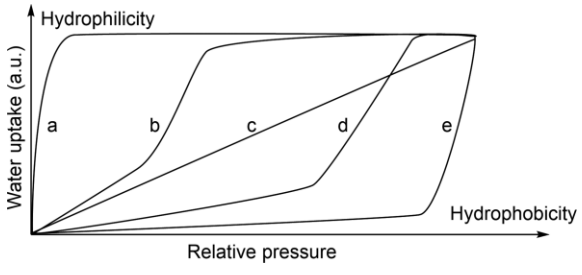

Figure 6. Comparison of different types of water adsorption isotherms. a: hydrophilic and microporous (e.g. zeolites); b: less hydrophilic, microporous (e.g. SAPO/AlPOs, hydrophilic MOFs); c) moderate hydrophilicity, amorphous micro up to mesoporous (e.g. mesoporous silica gels), d) hydrophobic, mesoporous; e) very hydrophobic (e.g. active carbon and related materials). For the version of this diagram with specific examples the reader is directed to Figure 4 in ref.[36] and to ref.[52] Noteworthy a microporous (regular density) silica gel has an isotherm of type I (a); however, less steep than a hydrophilic zeolite.

Stability of MOFs for Water Sorption

Water stability of MOFs is one of the necessary conditions for a sensible use in AHPs. For the use of MOFs in adsorption heat pumps, it is important to note that hydrothermal stability cannot be concluded by proving the structural integrity simply by immersing into and retrieving the MOF from an aqueous suspension. Instead, water stability needs to be verified through a larger number of water-vapor ad/desorption cycles (Figure 7).

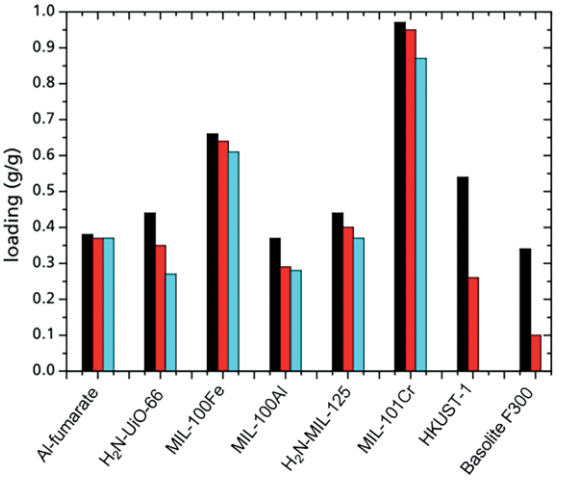

Figure 7. Water loading lift measured on Al fumarate,[82] H_2N-UiO-66,[81] MIL-100Fe,[67] MIL-100Al,[67] H_2N-MIL-125,[81] MIL-101Cr,[34] HKUST-1[35] and Basolite™ F300[35] after activation (black filled square), after 20 ad-/desorption cycles with water vapor (red filled square), and after 40 ad/desorption cycles (blue filled square). Graphic adapted from ref.[84] © (2014), with permission of the Royal Society of Chemistry.

Expected lifetimes in real adsorption-driven heat pumps are over 100,000 ad- and desorption-cycles.[35,77] The 100,000 cycles correspond to an estimate of ten years of operation in a heat pump.[77] Cycling water sorption over thousands of cycles will be impossible without very high water stability. The desired water stability depends on the metal and ligand building blocks. Stability is divided into thermodynamic and kinetic stability.[76,90,91] MOFs are 2- to 3-dimensional coordination compounds with the same stability principles which are known for molecular metal-ligand complexes. The coordinative metal-ligand bond can be viewed as a superposition of an ionic and a covalent bond. The ionic bond derives from the Coulomb interaction between a metal cation and a ligand anion or the negative end of a polar ligand molecule. A covalent metal-ligand sigma bond can be viewed as a Lewis acid (metal) –

Lewis base (ligand) (or acceptor–donor) interaction where a ligand donor atom donates its free electron pair into an empty metal orbital.

Water can react with metal-ligand complexes as a protic reagent (an acid) or as a ligand. Consequently, non-water-stable MOFs decompose either through hydrolysis or linker exchange. In the case of hydrolysis, the metal-ligand bond is broken with formation of the metal-hydroxide and the conjugated acid of the ligand.[92] During ligand exchange, a water molecule (an aqua ligand) replaces the original ligand.

$$M^{n+}\text{–}O_2C\text{-}R + H_2O \longrightarrow M^{n+}\text{–}OH + R\text{-}CO_2H$$

$$M^{n+}\text{–}O_2C\text{-}R + H_2O \longrightarrow M^{n+}\text{–}OH_2 + R\text{-}CO_2^-$$

The metal-ligand stability in terms of complex formation constant is determined by the metal cation and the ligand in equilibrium with the metal-ligand complex. The thermodynamic stability towards water can, in principle, be derived from this complex formation constant, the formation constant for the aqua-metal complex, the formation constant (or solubility product) for the hydroxido-metal complex (or metal hydroxide), and the pK_a value of the conjugated acid-base pair of the ligand. More practical, a higher covalency of the metal-ligand bonds is often viewed to go along with increased water stability. For example, azolates such as imidazolates have higher-lying nitrogen donor orbitals which are closer in energy to the empty metal orbitals and, thereby, give more covalent metal-nitrogen ligand bonds. Whereas carboxylates with their more electronegative oxygen donors yield to more ionic metal-ligand interactions. Consequently, ZIFs, where Zn2+ and imidazolate derivatives are combined, are rationalized more hydrolytically stable than MOF-5 analogs from Zn^{2+} and aryl-dicarboxylate ligands.[89,90,92] To a large extent the often noted hydrolytic stability of ZIF-8 is purely kinetic and due to the hydrophobicity of the material with almost no water uptake.[93,94] When the hydrophobicity/hydrophilicity of ZIF-8 was adjusted through linker modification as demonstrated by Zhang et al.[95] MAF-4 (ZIF-8, zinc 2-methylimidazolate) was tuned to become more hydrophilic by partial or full replacement of the linker with 3-methyl-1,2,4-triazolate in MAF-7. Replacing a C–H moiety with an isoelectronic N atom influenced the polarity of the resulting MOF strongly, where the additional N atom served as an extra adsorption site for polar water molecules.[35,95] This MAF-4 to –7 variation demonstrated the potential of MOF tailoring through partial isoreticular linker replacement (see below) but the more hydrophilic MAF-5 to –7 were no longer water stable. Figure 8 compares the water stability of different MOFs.

Qualitatively, also the HSAB concept allows a quick estimate of the bond strength. Soft acids, that are easily polarizable large metal cations in combination with low oxidation states will give stable combinations with soft bases, that are easily polarizable ligands.[89] Such soft acid–soft base interactions are orbital controlled and have a higher covalency than charge-controlled (more ionic) hard acid–hard base interactions between metal ions and ligand donor atoms of low polarizability.[76,89,90]

Besides or instead of thermodynamics, kinetics can be used to stabilize a material. In thermodynamics the Gibbs free energy (ΔG) determines stability/instability. Kinetic stability, that is inertness/lability of a compound, e.g. of a metal complex towards ligand exchange is concerned with the reaction rate (constant) and activation energy for the process. Even if a complex is thermodynamically unstable it can be kinetically inert. The well-known rate constants for the exchange of aqua ligands in aqua complexes $\{[M(H_2O)_n]^{c+} + H_2O^* - k(H_2O) \rightarrow [M(H_2O)_{n-1}(H_2O^*)]^{c+} + H_2O\}$ can be used to assess metal cations as inert or labile.[96–98] The divalent transition-metal cations from Mn^{2+} to Cu^{2+} have fast rate constants $k(H_2O)$ of over 10^6 s^{-1} for this exchange which renders their complexes rather labile. For trivalent Cr^{3+} $k(H_2O)$ is about 10^{-6} s^{-1} and Cr^{3+} complexes are generally viewed as inert. The most inert main-group metal-aqua complex is $[Al(H_2O)_6]^{3+}$ with $k(H_2O) = 1.3$ s^{-1}. Hence, Cr(III)- and Al(III)-MOFs are reasonably kinetically stable materials for AHPs. Along these lines, also Zr^{4+} and Ti^{4+} MOFs are among the more kinetically stable systems.

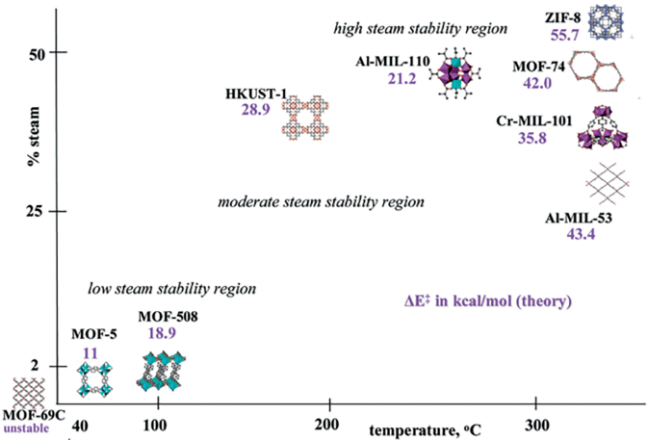

Figure 8. Hydrothermal stability of different MOFs against water vapor at different temperatures as a steam-temperature diagram. The corresponding activation energies for the MOFs, which are required for the exchange of a linker, are plotted as numerical values. Reproduced from ref.[92] © (2009), with permission from the American Chemical Society.

For MOFs, essentially three ways are discussed through which the hydrothermal decomposition can be kinetically inhibited. This includes steric shielding of the labile metal-donor atom bond, the increase of the material's hydrophobicity, and the use of rigid, inflexible linkers and metal-cluster secondary building units, SBUs.[89,76,90,92] Rigid linkers and SBUs significantly reduce linker exchange, while steric shielding makes the labile metal-linker bonds difficult to access for water molecules. The approach of hydrophobicity increase distinguishes between internal and external hydrophobicity. In the case of internal hydrophobicity, functionalization of the linker with e.g. fluorine atoms or alkyl chains slows down the approach of water molecules to the metal-linker bond. External hydrophobicity, on the other hand, prevents water molecules from penetrating into the pores of the material.[89,76]

The difference between the stability towards liquid water and towards water vapor in ad/desorption cycles can be explained by the water phase change enthalpy, the head of adsorption which is released at the adsorption site, i.e., in the MOF. Such adsorption enthalpies have been calculated to lie in the range of ligand displacement energies. In addition, water

molecules are constantly moved in and out of the porous material during cyclic ad/desorption processes. This increases the chance of metal-ligand bond hydrolysis and stresses the framework by the alternating forces created through cavitation (moving in) and capillary forces (moving out). For example, the Zr-MOF UiO-67 was shown to be stable towards linker hydrolysis in H_2O, but collapses during activation, that is desorption of H_2O from the pores through capillary-force-driven channel collapse.[99]

Linker Functionalization for Increased Hydrophilicity

A possibility to increase the hydrophilicity of a MOF is the functionalization of the aromatic spacer on the linker with an amino group. The amino-aryl function provides hydrogen-bond donor sites and thus an increased affinity of the MOF for water.[81,84] When UiO-66 and MIL-125 with their non-functionalized terephthalate linkers (O_2C-C_6H_4-CO_2) were compared to the analogs H_2N-UiO-66 and H_2N-MIL-125 with the 2-amino-terephthalate linker (O_2C-$C_6H_3(NH_2)$-CO_2)[81] the amino-functionalized MOFs showed a water uptake at lower p/p_0 (Figure 9). H_2N-MIL-125 also exhibited an extremely promising adsorption isotherm with the steep S-rise between 0.1 and 0.2 (p/p_0) being ideal for use in heat pumps. At the same time, H_2N-MIL-125 was shown to be stable to hydrolysis in over 40 water sorption cycles (Figure 9).

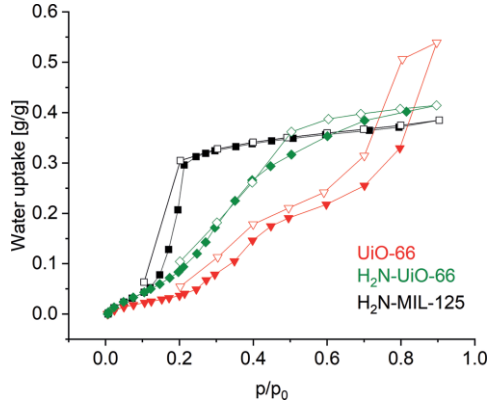

Figure 9. Water adsorption/desorption isotherms of UiO-66 (red), H_2N-UiO-66 (green) and H_2N-MIL-125 (black), acquired at T = 25 °C.[81] Adsorption: filled symbols; desorption: empty symbols.

Mixed Linker

In addition to functionalization, it is also possible to modulate the hydrophilicity or hydrophobicity of MOFs by using mixed linker systems. For example, Schlüsener et al. recently investigated a "solid solution" mixed-linker approach for aluminum MOFs.[100,101] Aluminum MOFs are particularly promising for industrial applications because aluminum salts are low cost and readily available starting materials, and their MOFs are rather hydrothermally robust materials which can also be manufactured in an environmentally friendly aqueous and even continuous route.[78,82,83,102,103] Schlüsener et al. were able to modulate the hydrophilicity between the two water-stable MOFs CAU-10-H and MIL-160 by varying the proportions of the two (commercially inexpensive) linkers (isophthalic acid and furandicarboxylic acid).

CAU-10-H[104] is currently the most realistic stable known MOF for hydrothermal cycling between 40 °C adsorption and 140 °C desorption temperature, with proven stability of 10,000 water adsorption-desorption cycles.[78] It has a BET surface area of over 1000 m^2/g and a water uptake of 0.33 g/g, even below the relative pressure of 0.2, which is significantly earlier than comparable MOFs.[105]

The tuning made it possible to continuously adjust the water adsorption in between the p/p_0 limits set by the two single-ligand MOFs. Figure 10 depicts the modulation of the hydrophilicity, i.e. the fine-tuning of the p/p_0 range of the water uptake step between MIL-160 and CAU-10-H thereby maintaining the single-step and high-uptake characteristics of the single-ligand starting MOFs.

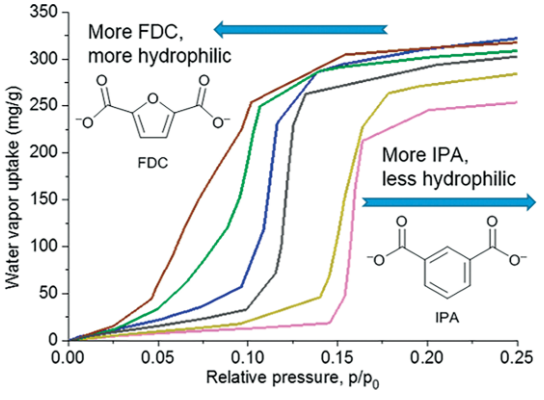

Figure 10. Fine-tuning of water adsorption curves with solid solution mixed-linker aluminum MOFs with varying furandicarboxylate and isophthalate linker proportions between (from left to right) neat MIL-160 (FDC-only, brown), IPA:FDC 22:78 (green), 53:47 (blue), 74:26 (grey), 85:15 (olive), neat CAU-10-H (IPA only, pink).[101] Reproduced from ref.[81] © (2019), with permission the American Chemical Society.

The above mixed-linker approach was only successful because of the very close isostructural MOF frameworks of MIL-160 and CAU-10-H. An only superfluous structural similarity may not be sufficient to yield such mixed-linker solid solution materials. Such was the case with the attempt to tune the water uptake between the MOFs CAU-23 (with 2,5-thiophenedicarboxylate, TDC) and MIL-160 (with FDC).[101] This attempt was made as CAU-23[106] and MIL-160[107,108] are seen as two of the most promising adsorbents for heat transformation.

All of the aforementioned Al-MOFs share fourfold helical chains of bis-OH and tetrakis-CO_2 bridged $\{Al(OH)_2(O–C–O)_4\}$ -polyhedra as the inorganic building unit, which are interconnected by the linkers to the 3D framework structures with square-shaped one-dimensional channels. The slight and easily overlooked difference lies in the or *cis*-$(OH)_2$ and *trans*-$(OH)_2$ connection of the $\{Al(OH)_2(O–C–O)_4\}$ octahedra which in turn depends on the opening angle between the di-carboxyl groups (Scheme 1).

MIL-160 and CAU-10-H, which enable the formation of solid solution mixed-linker networks, share the *cis*-$(\mu\text{-}OH)_2$ connectiv-

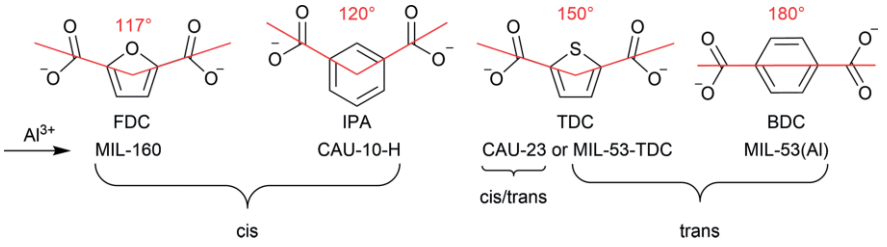

Scheme 1. Schematic illustration of linker molecules relevant in this work, their opening angles, and the resulting MOFs with their *cis*- and/or *trans*-$(\mu\text{-OH})_2$ connectivity of the $\{Al(OH)_2(O–C–O)_4\}$ octahedra.

ity of the $\{Al(OH)_2(O–C–O)_4\}$ octahedra. CAU-23 on the other hand features *cis*- and *trans*-connected $\{Al(OH)_2(O–C–O)_4\}$ along the chain. There is also a polymorph to CAU-23 in the form MIL-53-TDC with trans-only OH-bridges.[109] MIL-53-TDC also exhibits highly interesting water sorption properties with high hydrothermal stability and a favorable low isosteric heat of adsorption and a driving heat (for regeneration) below 65 °C.[110]

The different cis or trans connectivity of the infinite $\{Al(\mu\text{-OH})(O_2C\text{-})\}$ SBU apparently prevented the formation of clearly identifiable mixed-linker MOFs. Consequently, the three MOFs MIL-160, CAU-23, and MIL-53-TDC, which differ in *cis* and *trans* connectivity in their SBUs (Scheme 1), do not lead to a solid solution as in the case of CAU-10-H and MIL-160, but to mixed-MOF phases that are present side by side as in a physical mixture. The verification of mixed-MOF vs. mixed-linker proved, however, difficult since the differentiation via powder X-ray diffractometry (PXRD), IR-spectroscopy, and nitrogen sorption was either not conclusive enough or impossible, due to similarities (in PXRD) of the neat MOF phases. It was the curvature of the water sorption isotherms which indicated the simultaneous formation of the different MOF phases (albeit do not fully exclude mixed-linker MOFs which may form at low levels of substitution). Depending on the number and the position of the uptake steps, the different MOF phases could be discerned (Figure 11). Noteworthy, the MOF mixtures were obtained in-situ from one-pot syntheses of different linker mixtures. The resulting MOF mixtures then exhibited two or three uptake steps in their water sorption isotherms, corresponding to an overlay from the individual water sorption isotherms of MIL-160 (inflection point $p/p_0 \approx 0.07$), CAU-23 ($p/p_0 \approx 0.26$), and MIL-53-TDC ($p/p_0 \approx 0.33$) (Figure 11). The third water uptake step after 0.30 p/p_0 for MIL-53-TDC, was especially pronounced for the mixed-MOF material which was prepared from a 1:1 mixture of FDC and TDC. This was somewhat remarkable as the synthesis of MIL-53-TDC was hitherto unknown from purely aqueous synthesis conditions.[100]

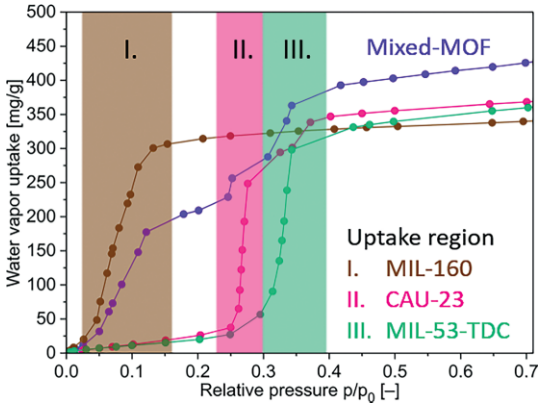

Figure 11. Comparison of uptake regions and water uptake from MIL-160, CAU-23, MIL-53-TDC, and the Mixed-MOF (purple-blue), containing a near 1:1 mixture of the TDC and FDC linker.[100] Reproduced from ref.[80] © (2019), with permission from the Royal Society of Chemistry.

Shaping

The shaping of the material is a necessary condition for the successful commercial application of MOFs. Traditionally, MOFs are obtained in the synthesis as microcrystalline powders, which in this form cannot be used or can only be used poorly in applications or devices. Suitable dosage forms for industrial applications are, for example, pellets, granules, monoliths, or membranes.[12,111–114]

The integration of porous materials in AHP devices requires close contact with a (metal) heat exchanger for the efficient and rapid dissipation of the heat of adsorption ($Q_{out,1}$) and the driving heat (Q_{drive}). Any increase in temperature within the sorption material during the working cycle (Figure 3) counteracts the desired uptake of the adsorbate. The close contact can be achieved by using a bulk of loose grains filled between the lamellae of a heat exchanger (Figure 12), by using monolayers of grains fixed/glued to the surface of the heat exchanger, by using binder coatings of small material particles or by using direct crystallization e.g. through partial support transformation into the porous material. For the latter three cases, the long-term mechanical stability is critical and must be ensured.[115,116] Although the latter three alternatives to fixed bed heat exchangers are more efficient, the fixed-bed technique is common because of its simplicity and its long-term mechanical stability.

In a proof-of-principle study, Gökpinar et al. prepared millimeter-scaled grains ca. 2 mm diameter of the Al-MOFs MIL-160 and Al-fumarate through the freeze granulation method (Figure 12) together with a pelleting device. Aluminum fumarate (Al-fum, commercially known as Basolite™ A520) is a very affordable MOF to manufacture. It is made at 60 °C from fumaric acid and (almost) any Al^{3+}salt sources in aqueous solution.[117] The BET surface area is around 1000 m^2/g and the water uptake is around 0.35 g/g. These properties, combined with an adsorption range at 0.2–0.3 relative pressure, make aluminum fumarate a suitable candidate for replacing silica gels in heat and cold applications. In addition, aluminum is stable over more

Minireview
doi.org/10.1002/ejic.202000834

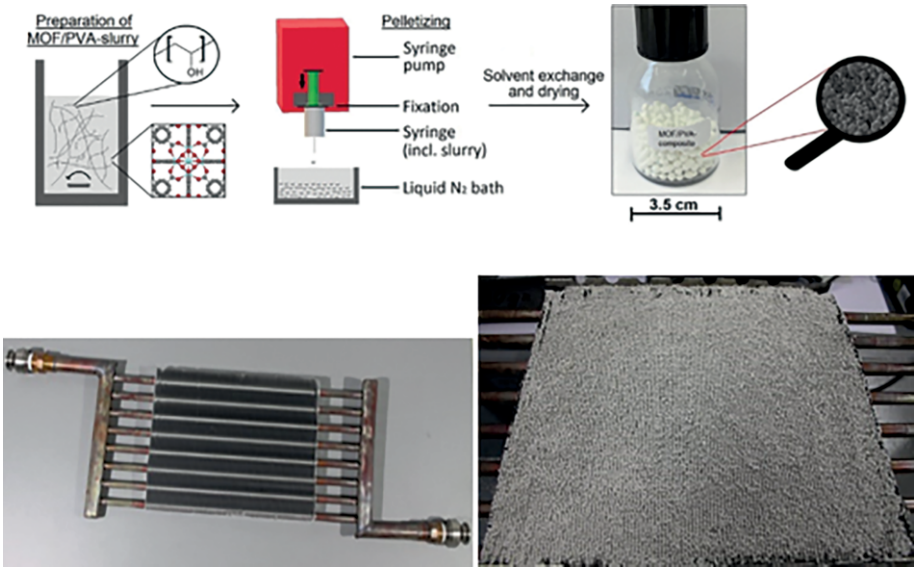

Figure 12. Top: freeze granulation process of MOF/polyvinyl alcohol (PVA) composites. Bottom: pipe-lamella heat exchanger unfilled (left) and filled (right) with pellets.[31] Reproduced from ref.[30] © (2019), with permission from the American Chemical Society.

than 4500 ad- and desorption cycles and has already been successfully tested in a heat pump prototype.[118] Poly(vinyl alcohol) (PVA) as binder gave highly mechanical and water stable, uniformly shaped MOF/PVA grains with 80 wt.-% MOF loading where the porosity properties of the MOFs were retained as verified by water adsorption isotherms, over 1000 water adsorption/desorption cycles and thermal and mechanical stability tests. The pellets withstood mechanical loads of up to 79 N. The Al-fumarate/PVA pellets were placed between the lamellae of a pipe-lamella heat exchanger, Dynamic adsorption and cooling performance testing provided specific cooling powers (SCP) from 349 up to 431 W/kg(adsorbent), which is better than current commercially used silica gel grains in AHPs under comparable operating conditions.[31]

Another promising shaping method for MOF/polymer monoliths was presented by Hastürk et al.[119,120] based on Sun's method of phase separation (Figure 13).[121] The Al-fum/PVA composites with a MOF loading of 50 to 80 wt.-% even exhibited an increased porosity. which was traced to additional mesopores from interfacial voids which were formed between Al-fum-particles and the PVA polymer. This additional interfacial volume leads in turn to an increase in water uptake capacity compared to the neat/pure MOF. The composites obtained had mechanical stability up to 63 N.

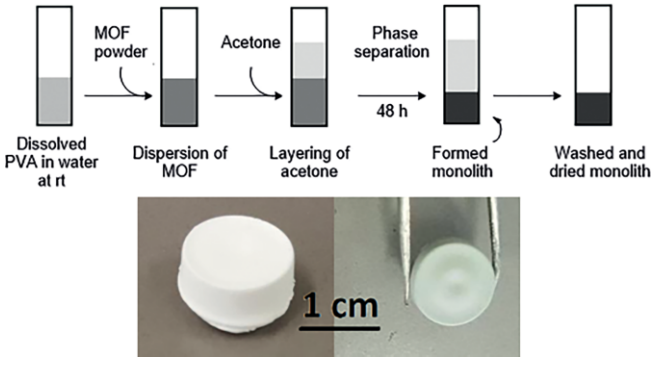

Figure 13. Top: schematic fabrication procedure of MOF/PVA monoliths via phase separation. Bottom: photographic images of Al-fum50/PVA2 (left) and MIL-101(Cr)40/PVA1 monolith (right).[120] Reproduced from ref.[100] © (2019), with permission from Elsevier.

Application

Meanwhile, many different methodologies have been envisioned for metal-organic frameworks suitable for water adsorption applications. These can roughly be divided into closed and open cycles.

Depending on the working mode (chiller or heat pump), different temperature levels are used and the efficiency, the so-called Coefficient of Performance (COP), can be defined differently. In both cases, the effort to spend is Q_{drive}. It is very important to note that the COP values vary with the working conditions, that is the adsorption temperature, condenser temperature, and evaporator temperature which in turn are chosen according to the sorption properties of the adsorbent-adsorbate working pair.[37]

In the heat pump mode, $Q_{out,1}$ and $Q_{out,2}$ are used for heating applications like floor heating or radiators. In this case, Q_{in} is the heat of evaporation that has been taken up from the environment, for instance by an earth probe.

The COP for the heat pump mode (COP_{HP}) is defined by:

$$COP_{HP} = \frac{-(Q_{out,1} + Q_{out,2})}{Q_{drive}}$$

In the chiller mode, a surrounding is cooled by evaporation of the working fluid and Q_{in} constitutes the useful cold, whereas the heat on medium temperature levels ($Q_{out,1}$ and

$Q_{out,2}$) has to be rejected to the environment. The COP for the chiller mode (COP_{Ch}) is defined by:

$$COP_{Ch} = \frac{Q_{in}}{Q_{drive}}$$

The COP_{Ch} values range from zero to less than 1 and COP_{HP} values range from one to less than two.[36] Chillers have already been commercialized, for instance by the companies Fahrenheit and Invensor. These systems reach COPs up to 0.75 (Invensor LTC 90e Plus). The adsorbents used in these systems are typically silica gel or a zeotype like SAPO-34.

Besides the efficiency or COP, the power and even more the power density of a heat transformation device is of major importance. Usually, the power *P* is defined as the ratio of mean heat gained over a half cycle (Q_{ads}) per half-cycle time (t_{cyc}):

$$P = \frac{Q_{ads}}{t_{cyc}}$$

The power density can be defined either with respect to the volume or to the mass. However, when presenting these values, the reference system (material, adsorber, module•••) has to be provided.

Open Cycles

When it comes to open cycles, there are two major applications: In thermal heat storage, waste heat is used to charge the storage by desorption of the adsorbent. As soon as heat is to be used, the storage can be discharged by a humid air stream flowing through the adsorbent bed. The performance, ecological and economic efficiency is highly dependent on the number of cycles per year due to heat losses.[122,123]

The other main application is air conditioning, for instance, drying of industrial process air (e.g. clean room) or air conditioning in non-residential buildings. For the latter, a comfort zone is defined in DIN EN 12779. The minimum and maximum temperatures and humidities herein are 20 to 26 °C and 30 to 65 % r.h. This comfort zone is depicted in Figure 14 in a Mollier diagram (light blue area). The target state of the ingoing air is usually at around 18 °C and 8 g kg^{-1}. In conventional systems, emanating from typical summer conditions (red circle, 35 °C and 15 g kg^{-1}) this state is reached by first cooling the air to the saturation line, then dehumidifying the air by condensation and finally heating of the air.

A most elaborated adsorption air conditioning process is the so-called *desiccant and evaporative cooling* (DEC) process (Figure 14, dashed line). In such a process, the ingoing air is dehumidified by an adsorbent and simultaneously heated by the released heat of adsorption (1 → 2), precooled by the air that comes from the building (2 → 3) and then humidified and

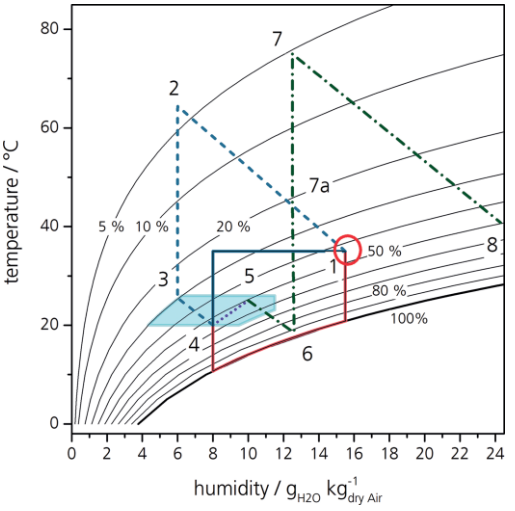

Figure 14. Process paths of a solid desiccant cooling (SDC) system (″) and of a desiccant and evaporative cooling (DEC) system (•: ingoing air, —: outgoing air) are depicted in comparison to a conventional A/C system (″) in a Mollier-diagram.

adiabatically cooled (3 → 4). The air coming from the building is first adiabatically cooled (5 → 6) and then used to precool the ingoing air (6 → 7a). In the last step the air is heated (7a → 7) and used for the regeneration of the adsorbent (7 → 8).[124] Power and efficiency of this process are mainly determined by the heat of adsorption and the necessary desorption temperature.[128]

In the aforementioned processes, the temperature boundaries are set by the application and humidities that are listed in Table 1 and plotted transferred to relative pressures in Figure 15. The colored areas show the working windows for the different applications. Therefore, an adsorbent has to be chosen according to the application. The necessary properties of an adsorbent are high uptake within the boundaries and stability against thermal and adsorption induced stress. The uptake capacity depends on geometrical parameters like pore volume and specific surface as well as on surface chemistry.

A great effort has been spent finding materials that match the different boundary conditions and has lately been exhaustingly reviewed.[76] Amongst the above mentioned metal-organic frameworks, MIL-160(Al) has been evaluated as a promising material for heat transformation and storage.[105,108] The work of Schlüsener and co-workers demonstrated the possibilities to tune the adsorption characteristics by a mixed linker approach varying the linker from furandicarboxylic acid to isophthalic acid yielding a mixture of MIL-160 and CAU-10-H structure.[101] These mixed-linker materials can be used at the standard conditions (evaporator temperature of 10 °C; mid. T of 40 °C) applying lower desorption temperatures. Therefore, these

Table 1. Boundary temperatures for open and closed thermally-driven applications.

	closed			open	
	Heat pump	Chiller	Server cooling	Heat storage	Dehumidification
Evaporator	–10–15 °C	–15–25 °C	18–22 °C	–10–22 °C	8–17 °C
Adsorber/Condenser	35–65 °C	20–37 °C	27–32 °C	25–100 °C	30–50 °C
Desorption	95–250 °C	55–95 °C	55–65 °C	100–250 °C	50–95 °C

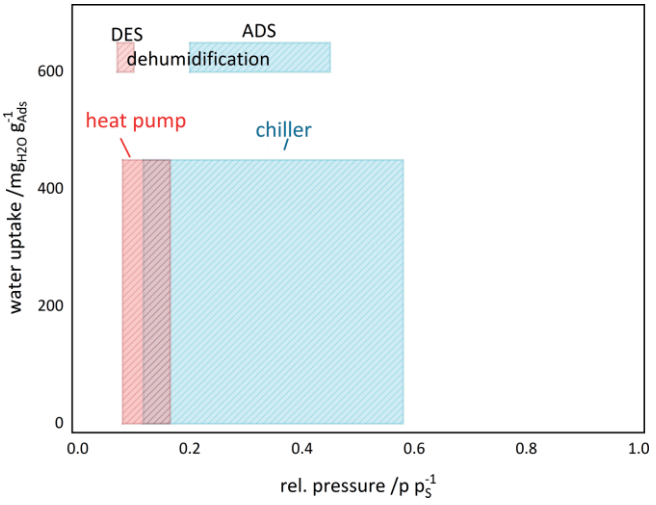

Figure 15. Working windows of possible application based on water adsorption.

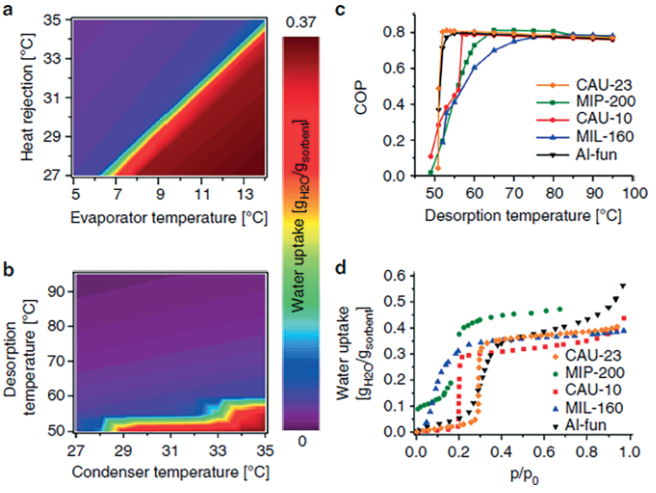

Figure 16. Calculation of adsorption driven chiller temperature boundaries for CAU-23 and coefficient of performance for cooling in comparison with selected state of the art materials. Calculated loading of CAU-23 for different temperatures used in an ADC setup for adsorption **a**, and desorption cycle **b**. Calculation of the COP values for different driving temperatures (assumed desired cooling of 10 °C and back cooling temperature of 30 °C). **d** Water adsorption curves at 40 °C of selected compounds. Reproduced from ref.[106] © (2019), with permission from Springer Nature.

materials show higher COP values at lower desorption temperatures.

Since water has the disadvantage of freezing at temperatures below 0 C, methanol has been investigated as a possible working fluid with HKUST-1 and MIL-101(Cr) showing COP-values higher than 1 for evaporator temperatures below 0 °C and adsorption temperatures between 40 °C and 50 °C. Later, MIL-53-muc was shown to yield a COP_{HP} of over 1.6 for evaporator temperatures of 0 °C and of almost 1.4 for evaporator temperatures of –10 °C by researchers of the Janiak group.[126–129]

The same MOF has also been evaluated for the use in adsorption chillers with a COP_{CH} of over 0.7 at ice-making conditions surpassing the performance of activated carbon/methanol.[129–134]

When it comes to adsorption chillers, metal-organic frameworks fully develop their potential due to their well-balanced hydrophilicity and the possibility to adjust the adsorption characteristics according to the application. An impressive example is the development of MIL-53-TDC showing sufficient water uptake capacities of 0.35 g•g^{-1} for comparably high evaporation temperatures of above 15 °C and/or heat rejection below 30 °C. At this condenser temperature, the MOF can be fully dried at desorption temperatures of only 60 °C.[110] This development pathed the way towards MOFs for ultra-low temperature-driven cooling yielding in the isostructural MOF CAU-23 As can be seen from Figure 16 this MOF yields a very high cooling COP_{Ch} of 0.8 at ultra-low temperature of less than 55 °C and typical cooling conditions of 10 °C and 30 °C.[106] (Figure 16).

Thermal batteries can be seen as a sub-category of thermal heat storage based on a closed cycle. The working principle is described in detail elsewhere.[135–137] The targeted performance as defined by the U.S. Department of Energy is a minimum heat storage capacity of 2.5 kW h with the condition of the maximum weight of the heat exchanger system of 35 kg.[138] Just recently, a composite material of LiCl@UiO-66 has been proven to be able to fulfil the capacity by use of only 10 kg of this material outperforming the benchmark material up to this date.[139]

Conclusions

With their high-water adsorption capacity, MOFs can significantly expand the existing inorganic sorption materials for heat transformation applications through the cycling ad- and desorption of water. The water adsorption behavior of MOFs can be controlled by the hydrophilic nature of the linker, i.e. the organic bridging ligand. On the way to a mature application, further optimizations of the kinetics of water sorption and the proof of hydrothermal stability for more than 100,000 adsorption and desorption cycles are necessary. In place of water, alcohols are also possible working fluids, thus extending the range of MOFs that can be used. Some MOFs are already industrially produced today (e.g. by BASF and marketed under the name Basolite™). A current challenge is still the processing of MOFs into shaped parts and the deposition and adherence of MOFs on surfaces. By solving these challenges, heat and mass transfer can be further improved, making MOFs sought-after new materials for numerous future tasks in heat transformation and storage, but also catalysis, gas separation, and storage.

Outlook and Future Challenges

As shown within this review, the development of materials made a great success, and a lot of great materials have been identified showing steep water uptake curves within the whole area of relative pressures, also techniques have been proposed to further shape the water uptake curves. To push these materials further towards the application, the research should be oriented on the application. New materials usually make it into the application when they either come with a new function or they fulfil a needed task better or cheaper as compared to state-of-the-art materials. In the case of MOFs for heat transformation, MOFs have to compete with activated carbon, silica

gel, and zeotypes, all well researched and developed materials. Although further work should be invested to decrease the synthesis effort of MOFs, they might never become competitive to silica gels or zeolites in terms of cost per mass of dry powder. Also, when it comes to comparing the volumetric loading (water mass uptake per *volume* of adsorbent, e.g. kg m^{-3}) or to power density (generated heating or cooling power per *volume* of adsorbent, e.g. kW m^{-3}) MOFs are only partly competitive to commercial silica gels due to the low specific density of MOFs.[140] Therefore, MOFs have to become more competitive in terms of cost per (volume) specific power. This may either be achieved by adjusting material characteristics in terms of higher uptake per volume of MOF or by improving heat and mass transfer by optimized shaping technologies. When it comes to shaping, it would be beneficial to provide a solution that can be employed in existing technologies easily, leading to either (directly) coated heat exchangers or granules in the size of silica gel granules that can be glued on heat exchanger structures with established approaches.

To further ensure the long time stability, the stability should be within the focus of further research not only in the case of hydrothermal cycles but also in the case of compatibility of the MOFs in combination with a supporting structure like the heat exchanger materials, binding agents, and the working fluids. Here, issues like outgassing, adhesion, fouling, corrosion, and decomposition have to be further understood and taken care of.

Last but not least, life cycle analyses are under-presented in this field, especially taking into account that the technology of heat transformation is intended to save CO_2. Profound LCA studies starting at the synthesis of MOFs and taking also into account the full operating lifetime will definitely be guiding further needs for research and development.

Acknowledgments

Funding by the German Federal Ministry of Economics (BMWi) for the project Nextsol under grant-# 0327851A/B and by the German Federal Ministry of Education and Research (BMFT) for the project Optimat under grant 03SF0492A/C is gratefully acknowledged. Open access funding enabled and organized by Projekt DEAL.

Keywords: Adsorption-driven heat pumps · Adsorption heat transformation · Metal-organic frameworks · Sorption materials · Water sorption

[1] S. R. Batten, N. R. Champness, X.-M. Chen, J. Garcia-Martinez, S. Kitagawa, L. Öhrström, M. O'Keeffe, M. Paik Suh, J. Reedijk, *Pure Appl. Chem.* **2013**, *85*, 1715–1724.
[2] C. Janiak, *Dalton Trans.* **2003**, 2781–2804.
[3] C. Janiak, J. K. Vieth, *New J. Chem.* **2010**, *34*, 2366–2388.
[4] A. Schoedel, S. Rajeh, *Top. Curr. Chem.* **2020**, *378*, 19.
[5] J. D. Evans, B. Garai, H. Reinsch, W. Li, S. Dissegna, V. Bon, I. Senkovska, R. A. Fischer, S. Kaskel, C. Janiak, N. Stock, D. Volkmer, *Coord. Chem. Rev.* **2019**, *380*, 378–418.
[6] H.-C. Zhou, S. Kitagawa, *Chem. Soc. Rev.* **2014**, *43*, 5415–5418.
[7] J. R. Long, O. M. Yaghi, *Chem. Soc. Rev.* **2009**, *38*, 1213–1214.
[8] R. B. Getman, Y.-S. Bae, C. E. Wilmer, R. Q. Snurr, *Chem. Rev.* **2012**, *112*, 703–723.
[9] K. Adil, Y. Belmabkhout, R. S. Pillai, A. Cadiau, P. M. Bhatt, A. H. Assen, G. Maurin, M. Eddaoudi, *Chem. Soc. Rev.* **2017**, *46*, 3402–3430.
[10] J. Dechnik, C. J. Sumby, C. Janiak, *Cryst. Growth Des.* **2017**, *17*, 4467–4488.
[11] J. Dechnik, J. Gascon, C. J. Doonan, C. Janiak, C. J. Sumby, *Angew. Chem. Int. Ed.* **2017**, *56*, 9292–9310; *Angew. Chem.* **2017**, *129*, 9420.
[12] H. B. Tanh Jeazet, C. Staudt, C. Janiak, *Dalton Trans.* **2012**, *41*, 14003–14027.
[13] A. Nuhnen, D. Dietrich, S. Millan, C. Janiak, *ACS Appl. Mater. Interfaces* **2018**, *10*, 33589–33600.
[14] M. A. Carreon, S. R. Venna "*Metal Organic Framework Membranes for Molecular Gas Separations*". Vol 6, World Scientific**. 2020**.
[15] S. M. J. Rogge, A. Bavykina, J. Hajek, H. Garcia, A. I. Olivos-Suarez, A. Sepúlveda-Escribano, A. Vimont, G. Clet, P. Bazin, F. Kapteijn, M. Daturi, E. V. Ramos-Fernandez, F. X. Llabrés i Xamena, V. Van Speybroeck, J. Gascon, *Chem. Soc. Rev.* **2017**, *46*, 3134–3184.
[16] L. Wang, M. Zheng, Z. Xie, *J. Mater. Chem. B* **2018**, *6*, 707–717.
[17] W. Chen, C. Wu, *Dalton Trans.* **2018**, *47*, 2114–2133.
[18] X. Lian, Y. Fang, E. Joseph, Q. Wang, J. Li, S. Banerjee, C. Lollar, X. Wang, H.-C. Zhou, *Chem. Soc. Rev.* **2017**, *46*, 3386–3401.
[19] S. Cohen, *Chem. Sci.* **2010**, *1*, 32–36.
[20] O. K. Farha, A. Ö. Yazaydin, I. Eryazici, C. D. Malliakas, B. G. Hauser, M. G. Kanatzidis, S. T. Nguyen, R. Q. Snurr, J. T. Hupp, *Nat. Chem.* **2010**, *2*, 944–948.
[21] *World Economic Forum, Global Risks **2015***, 10th Edition (World Economic Forum, Geneva, Switzerland, **2015**, accessed Aug, 2020. http://www3.weforum.org/docs/WEF_Global_Risks_2015_Report15.pdf.
[22] M. M. Mekonnen, A. Y. Hoekstra, *Sci. Adv.* **2016**, *2*, 1500323.
[23] S.-I. Kim, T.-U. Yoon, M.-B. Kim, S.-J. Lee, Y. K. Hwang, J.-S. Chang, H.-J. Kim, H.-N. Lee, U.-H. Lee, Y.-S. Bae, *Chem. Eng. J.* **2016**, *286*, 467–475.
[24] F. Trapani, A. Polyzoidis, S. Loebbecke, C. G. Piscopo, *Microporous Mesoporous Mater.* **2016**, *230*, 20–24.
[25] H. Kim, S. Yang, S. R. Rao, S. Narayanan, E. A. Kapustin, H. Furukawa, A. S. Umans, O. M. Yaghi, E. N. Wang, *Science* **2017**, *356*, 430-434.</jnl>
[26] M. S. Hanikel, F. Prevot, E. A. Fathieh, H. Kapustin, H. Lyu, H. Wang, N. J. Diercks, T. G. Glover, O. M. Yaghi, *ACS Cent. Sci.* **2019**, *5*, 1699–1706.
[27] A. J. Rieth, A. M. Wright, S. Rao, H. Kim, A. D. LaPotin, E. N. Wang, M. Dinca, *J. Am. Chem. Soc.* **2018**, *140*, 17591–17596.
[28] E. Elsayed, R. Al-Dadah, S. Mahmoud, A. Elsayed, P. A. Anderson, *Appl. Therm. Eng.* **2016**, *99*, 802–812.
[29] R. Al-Dadah, S. Mahmoud, E. Elsayed, P. Youssef, F. Al-Mousawi, *Energy* **2020**, *190*, 116356.
[30] K. Leus, T. Bogaerts, J. De Decker, H. Depauw, K. Hendrickx, H. Vrielinck, V. Van Speybroeck, P. Van Der Voort, *Microporous Mesoporous Mater.* **2016**, *226*, 110–116.
[31] S. Gökpinar, S.-J. Ernst, E. Hastürk, M. Möllers, I. El Aita, R. Wiedey, N. Tannert, S. Nießing, S. Abdpour, A. Schmitz, J. Quodbach, G. Füldner, S. K. Henninger, C. Janiak, *Ind. Eng. Chem. Res.* **2019**, *58*, 21493–21503.
[32] S. K. Henninger, F. P. Schmidt, H. M. Henning, *Appl. Therm. Eng.* **2010**, *30*, 1692–1702.
[33] C. Janiak, S. K. Henninger, *Chimia* **2013**, *67*, 419–424.
[34] J. Ehrenmann, S. K. Henninger, C. Janiak, *Eur. J. Inorg. Chem.* **2011**, 471–474.
[35] S. K. Henninger, F. Jeremias, H. Kummer, C. Janiak, *Eur. J. Inorg. Chem.* **2012**, *2012*, 2625–2634.
[36] M. F. de Lange, K. J. F. M. Verouden, T. J. H. Vlugt, J. Gascon, F. Kapteijn, *Chem. Rev.* **2015**, *115*, 12205–12250.
[37] D. B. Boman, D. C. Hoysall, D. G. Pahinkar, M. K. J. Ponkala, S. Garimella, *Appl. Therm. Eng.* **2017**, *123*, 422–434.
[38] J. Jänchen, D. Ackermann, H. Stach, W. Brosicke, *Solar Energy* **2004**, *76*, 339–344.
[39] F. P. Schmidt, S. K. Henninger, H. Stach, J. Jänchen, H.-M. Henning, *NoVel adsorbents for solar cooling applications*, Proceedings of the International Conference on Solar Air-Conditioning; OTTI Technology Kolleg: Staffelstein, **2005** (October 6/7); pp. 39–44.
[40] K. C. Ng, H. T. Chua, C. Y. Chung, C. H. Loke, T. Kashiwagi, A. Akisawa, B. B. Saha, *Appl. Therm. Eng.* **2001**, *21*, 1631–1642.

[41] S. K. Henninger, F. Jeremias, H. Kummer, P. Schossig, H.-M. Henning, *Energy Procedia* **2012**, *30*, 279–288.
[42] M. M. Younes, I. I: El-Sharkawy, A. E. Kabeel, B. B. Saha, *Appl. Therm. Eng.* **2017**, *114*, 394-414.
[43] A. Pal, K. Thu, S. Mitra, I. I. El-Sharkawy, B. B. Saha, H.-S. Kil, S.-H. Yoon, J. Miyawaki, *Int. J. Heat Mass Transfer* **2017**, *110*, 7–19.
[44] I. I. El-Sharkawy, K. Uddin, T. Miyazaki, B. B. Saha, S. Koyama, H.-S. Kil, S.-H. Yoon, J. Miyawaki, *Int. J. Heat Mass Transfer* **2015**, *81*, 171–178.
[45] S. Vasta, V. Brancato, D. La Rosa, V. Palomba, G. Restuccia, A. Sapienza, A. Frazzica, *Nanomaterials* **2018**, *8*, 522.
[46] H. T. Chua, K. C. Ng, A. Chakraborty, N. M. Oo, M. A. Othman, *J. Chem. Eng. Data* **2002**, *47*, 1177–1181.
[47] N. M. Voskresenskii, B. N. Okunev, L. G. Gordeeva, *Therm. Eng.* **2018**, *65*, 524–530.
[48] L. G. Gordeeva, A. Freni, T. A. Krieger, G. Restuccia, Y. I. Aristov, *Microporous Mesoporous Mater.* **2008**, *112*, 254–261.
[49] Y. I. Aristov, G. Restuccia, G. Cacciola, V. N. Parmon, *Appl. Therm. Eng.* **2002**, *22*, 191–204.
[50] A. Freni, G. Maggio, A. Sapienza, A. Frazzica, G. Restuccia, S. Vasta, *Appl. Therm. Eng.* **2016**, *104*, 85–95.
[51] S. K. Henninger, S.-J. Ernst, L. Gordeeva, P. Bendix, D. Fröhlich, A. D. Grekova, L. Bonaccorsi, Y. Aristov, J. Jaenchen, *Renewable Energy* **2017**, *110*, 59–68.
[52] Mitsubishi Plastics. Zeolitic Water Vapor Adsorbent: AQSOA. http://www.aaasaveenergy.com/products/001/pdf/AQSOA_1210E.pdf (accessed 05–12–2018).
[53] H. Kakiuchi S. Shimooka M. Iwade K. Oshima M. Yamazaki S. Terada, H. Watanabe, T. Takewaki, *Kagaku Kogaku Ronbunshu* **2005**, *31*, 273–277.
[54] H. Kakiuchi S. Shimooka M. Iwade K. Oshima, M. Yamazaki, S. Terada, H. Watanabe, T. Takewaki, *Kagaku Kogaku Ronbunshu* **2005**, *31*, 361–364.
[55] Y. H. H. Luo, J. L. Funke, R. D. Falconer, *Ind. Eng. Chem. Res.* **2016**, *55*, 9749–9757.
[56] B. B. Saha, E. C. Boelman, T. Kashiwagi, *ASHRAE Trans.* **1995**, *101*, 348–357.
[57] H. Wu, F. Salles, J. Zajac, *Molecules* **2019**, *24*, 945.
[58] J. M. S. Dias, V. A. F. Costa, *Renewable Sustainable Energy Rev.* **2018**, *98*, 317–327.
[59] F. Kuznik, K. Johannes, C. Obrecht, D. David, *Renewable Sustainable Energy Rev.* **2018**, *94*, 576–586.
[60] F. Shabir, M. Sultan, T. Miyazaki, B. B. Saha, A. Askalany, I. Ali, Y. Zhou, R. Ahmad, R. R. Shamshiri, *Renewable Sustainable Energy Rev.* **2020**, *119*, 109630.
[61] Z. Tamainot-Telto, S. J. Metcalf, R. E. Critoph, Y. Zhong, R. Thorpe, *Int. J. Refrig.* **2009**, *32*, 1212–1229.
[62] A. A. Askalany, B. B. Saha, *Heat Mass Transfer* **2017**, *53*, 107–114.
[63] A. A. Askalany, B. B. Saha, M. S. Ahmed, I. M. Ismail, *Int. J. Refrig.* **2013**, *36*, 1037–1044.
[64] E. J. A. Hu, *Sol. Energy* **1998**, *62*, 325–329.
[65] G. Férey, *Dalton Trans.* **2009**, 4400–4415.
[66] G. Akiyama, R. Matsuda, S. Kitagawa, *Chem. Lett.* **2010**, *39*, 360–361.
[67] F. Jeremias, A. Khutia, S. K. Henninger, C. Janiak, *J. Mater. Chem.* **2012**, *22*, 10148–10151.
[68] C. Janiak, S. K. Henninger, *Nachr. Chem.* **2013**, *61*, 520–523.
[69] H. A. Habib, J. Sanchiz, C. Janiak, *Dalton Trans.* **2008**, 1734–1744.
[70] S. K. Henninger, H. A. Habib, C. Janiak, *J. Am. Chem. Soc.* **2009**, *131*, 2776–2777.
[71] Y. Aristov, *J. Chem. Eng. Jpn.* **2007**, *40*, 1242–1251.
[72] J. Canivet, A. Fateeva, Y. Guo, B. Coasne, D. Farrusseng, *Chem. Soc. Rev.* **2014**, *43*, 5594–5617.
[73] J. Rouquerol, D. Avnir, C. W. Fairbridge, D. H. Everett, J. M. Haynes, N. Pernicone, J. D. F. Ramsay, K. S. W. Sing, K. K. Unger, *Pure Appl. Chem.* **1994**, *66*, 1739–1758.
[74] M. Thommes, K. Kaneko, A. V. Neimark, J. P. Olivier, F. Rodriguez-Reinoso, J. Rouquerol, K. S. W. Sing, *Pure Appl. Chem.* **2015**, *87*, 1051–1069.
[75] Y. I. Aristov, *Appl. Therm. Eng.* **2013**, *50*, 1610–1618.
[76] X. Liu, X. Wang, F. Kapteijn, *Chem. Rev.* **2020**, *120*, 8303–8377.
[77] E. Hastürk, S.-J. Ernst, C. Janiak, *Curr. Opin. Chem. Eng.* **2019**, *24*, 26–36.
[78] D. Fröhlich, E. Pantatosaki, P. D. Kolokathis, K. Markey, H. Reinsch, M. Baumgartner, M. A. van der Veen, D. E. De Vos, N. Stock, G. K. Papadopoulos, S. K. Henninger, C. Janiak, *J. Mater. Chem. A* **2016**, *4*, 11859–11869.
[79] A. Khutia, H. U. Rammelberg, T. Schmidt, S. Henninger, C. Janiak, *Chem. Mater.* **2013**, *25*, 790–798.
[80] T. J. Matemb Ma Ntep, H. Reinsch, B. Moll, E. Hastürk, S. Gökpinar, H. Breitzke, C. Schlüsener, L. Schmolke, G. Buntkowsky, C. Janiak, *Chem. Eur. J.* **2018**, *24*, 14048–14053.
[81] F. Jeremias, V. Lozan, S. K. Henninger, C. Janiak, *Dalton Trans.* **2013**, *42*, 15967–15973.
[82] F. Jeremias, D. Fröhlich, C. Janiak, S. K. Henninger, *RSC Adv.* **2014**, *4*, 24073–24082.
[83] D. Fröhlich, S. K. Henninger, C. Janiak, *Dalton Trans.* **2014**, *43*, 15300–15304.
[84] F. Jeremias, D. Fröhlich, C. Janiak, S. Henninger, *New J. Chem.* **2014**, *38*, 1846–1852.
[85] P. Kim, S. Agnihotri, *J. Colloid Interface Sci.* **2008**, *325*, 64–73.
[86] G. Wang, K. Leus, H. S. Jena, C. Krishnaraj, S. Zhao, H. Depauw, N. Tahier, Y.-Y. Liu, P. van der Voort, *J. Mater. Chem. A* **2018**, *6*, 6370.
[87] S. Dey, A. Bhunia, I. Boldog, C. Janiak, *Microporous Mesoporous Mater.* **2017**, *241*, 303–315.
[88] S. Dey, A. Bhunia, H. Breitzke, P. B. Groszewicz, G. Buntkowsky, C. Janiak, *J. Mater. Chem. A* **2017**, *5*, 3609–3620.
[89] O. M. Yaghi, M. J. Kalmutzki, C. S. Diercks, *Introduction to Reticular Chemistry. Metal-organic frameworks and covalent organic frameworks*, Wiley, Weinheim, **2019**.
[90] M. J. Kalmutzki, C. S. Diercks, O. M. Yaghi, *Adv. Mater.* **2018**, *30*, 1704304.
[91] N. C. Burtch, H. Jasuja, K. S. Walton, *Chem. Rev.* **2014**, *114*, 10575–10612.
[92] J. J. Low, A. I. Benin, P. Jakubczak, J. F. Abrahamian, S. A. Faheem, R. R. Willis, *J. Am. Chem. Soc.* **2009**, *131*, 15834–15842.
[93] K. Zhang, R. P. Lively, C. Zhang, W. J. Koros, R. R. Chance, *J. Phys. Chem. C* **2013**, *117*, 7214–7225.
[94] S. Tanaka, Y. Tanaka, *ACS Omega* **2019**, *4*, 19905–19912.
[95] J.-P. Zhang, A.-X. Zhu, R.-B. Lin, X.-L. Qi, X.-M. Chen, *Adv. Mater.* **2011**, *23*, 1268–1271.
[96] L. Helm, A. E. Merbach, *Coord. Chem. Rev.* **1999**, *187*, 151–181.
[97] L. Helm, G. M. Nicolle, A. E. Merbach, *Adv. Inorg. Chem.* **2005**, *57*, 327–379.
[98] S. E. Lincoln, *Helv. Chim. Acta* **2005**, *88*, 523–545.
[99] J. E. Mondloch, M. J. Katz, N. Planas, D. Semrouni, L. Gagliardi, J. T. Hupp, O. K. Farha, *Chem. Commun.* **2014**, *50*, 8944–8946.
[100] C. Schlüsener, D. N. Jordan, M. Xhinovci, T. J. Matemb, M. Nteb, A. Schmitz, B. Giesen, C. Janiak, *Dalton Trans.* **2020**, *49*, 7373–7383.
[101] C. Schlüsener, M. Xhinovci, S.-J. Ernst, A. Schmitz, N. Tannert, C. Janiak, *Chem. Mater.* **2019**, *31*, 4051–4062.
[102] N. Tannert, C. Jansen, S. Nießing, C. Janiak, *Dalton Trans.* **2019**, *48*, 2967–2976.
[103] M. Gaab, N. Trukhan, S. Maurer, R. Gummaraju, U. Müller, *Microporous Mesoporous Mater.* **2012**, *157*, 131–136.
[104] H. Reinsch, M. A. van der Veen, B. Gil, B. Marszalek, T. Verbiest, D. de Vos, S. Norbert, *Chem. Mater.* **2013**, *25*, 17–26.
[105] A. Cadiau, J. S. Lee, D. D. Borges, P. Fabry, T. Devic, M. T. Wharmby, C. Martineau, D. Foucher, F. T. Taulelle, C.-H. Jun, Y. K. Hwang, N. Stock, M. F. De Lange, F. Kapteijn, J. Gascon, G. Maurin, J.-S. Chang, C. Serre, *Adv. Mater.* **2015**, *27*, 4775–4780.
[106] D. Lenzen, J. Zhao, S.-J. Ernst, M. Wahiduzzaman, A. Ken Inge, D. Fröhlich, H. Xu, H.-J. Bart, C. Janiak, S. Henninger, G. Maurin, X. Zou, N. Stock, *Nat. Commun.* **2019**, *10*, 3025.
[107] A. Permyakova, O. Skrylnyk, E. Courbon, M. Affram, S. Wang, U.-H. Lee, A. H. Valekar, F. Nouar, G. Mouchaham, T. Devic, G. de Weireld, J.-S. Chang, N. Steunou, M. Frère, C. Serre, *ChemSusChem* **2017**, *10*, 1419–1426.
[108] A. Permyakova, S. J. Wang, E. Courbon, F. Nouar, N. Heymans, P. D'Ans, N. Barrier, P. Billemont, G. DeWeireld, N. Steunou, M. Frere, C. Serre, *J. Mater. Chem. A* **2017**, *5*, 12889–12898.
[109] C. B. L. Tschense, N. Reimer, C.-W. Hsu, H. Reinsch, R. Siegel, W.-J. Chen, C.-H. Lin, A. Cadiau, C. Serre, J. Senker, N. Stock, *Z. Anorg. Allg. Chem.* **2017**, *643*, 1600–1608.
[110] N. Tannert, S.-J. Ernst, C. Jansen, H.-J. Bart, S. K. Henninger, C. Janiak, *J. Mater. Chem. A* **2018**, *6*, 17706–17712.
[111] S. Kaskel, U.-H. Lee, A. H. Valekar, Y. K. Hwang, J.-S. Chang, *The Chemistry of Metal-Organic Frameworks, Synthesis, Characterization, and Application*, Wiley-VCH, Weinheim, **2017**, pp. 551–571.

[112] L. D. O'Neill, H. Zhang, D. J. Bradshaw, *J. Mater. Chem.* **2010**, *20*, 5720–5726.
[113] R. Ostermann, J. Cravillon, C. Weidmann, M. Wiebcke, B. M. Smarsly, *Chem. Commun.* **2011**, *47*, 442–444.
[114] S. Qiu, M. Xue, G. Zhu, *Chem. Soc. Rev.* **2014**, *43*, 6116–6140.
[115] A. Freni, L. Bonaccorsi, L. Calabrese, A. Caprì, A. Frazzica, A. Sapienza, *Appl. Therm. Eng.* **2015**, *82*, 1–7.
[116] A. Freni, B. Dawoud, L. Bonaccorsi, S. Chmielewski, A. Frazzica, L. Calabrese, G. Restuccia, *Characterization of Zeolite-Based Coatings for Adsorption Heat Pumps*; SpringerBriefs in *Applied Sciences and Technology* (Chapter 4); Springer, **2015**.
[117] E. Leung, U. Müller, N. Trukhan, H. Mattenheimer, G. Cox, S. Blei, Process for preparing porous metal-organic frameworks based on aluminum fumarate, US20120082864A1, **2012**.
[118] H. Kummer, F. Jeremias, A. Warlo, G. Füldner, D. Fröhlich, C. Janiak, R. Gläser, S. K. Henninger, *Ind. Eng. Chem. Res.* **2017**, *56*, 8393–8398.
[119] E. Hastürk, C. Schlüsener, J. Quodbach, A. Schmitz, C. Janiak, *Microporous Mesoporous Mater.* **2019**, *280*, 277–287.
[120] E. Hastürk, S.-P. Höfert, B. Topalli, C. Schlüsener, C. Janiak, *Microporous Mesoporous Mater.* **2020**, *295*, 109907.
[121] X. Sun, T. Fujimoto, H. Uyama, *Polym. J.* **2013**, *45*, 1101–1106.
[122] C. Rathgeber, E. Lavemann, A. Hauer, *J. Energy Storage* **2015**, *2*, 43–46.
[123] H. Schreiber, F. Lanzerath, C. Reinert, C. Gruntgens, A. Bardow, *Appl. Therm. Eng.* **2016**, *106*, 981–991.
[124] H.-M. Henning, T. Urbaneck, A. Morgenstern, T. Nunez, E. Wiemken, E. Thümmler, U. Uhlig, *Kühlen und Klimatisieren mit Wärme*, 2nd ed., Fraunhofer-IRB-Verlag, Stuttgart, **2015**.
[125] T. S. Ge, Y. J. Dai, R. Z. Wang, Y. Li, *Appl. Therm. Eng.* **2013**, *58*, 281–290.
[126] M. F. de Lange, B. L. van Velzen, C. P. Ottevanger, K. J. F. M. Verouden, L.-C. Lin, T. J. H. Vlugt, J. Gascon, F. Kapteijn, *Langmuir* **2015**, *31*, 12783–12796.
[127] S.-J. Ernst, F. Jeremias, H.-J. Bart, S. K. Henninger, *Ind. Eng. Chem. Res.* **2016**, *55*, 13094–13101.
[128] H. Kummer, M. Baumgartner, P. Hügenell, D. Fröhlich, S. K. Henninger, R. Gläser, *Appl. Therm. Eng.* **2017**, *117*, 689–697.
[129] T. J. Matemb Ma Nteb, H. Reinsch, P. P. C. Hügenell, S.-J. Ernst, E. Hastürk, C. Janiak, *J. Mater. Chem. A* **2019**, *7*, 24973–24981.
[130] R. E. Critoph, *Sol. Energy* **1988**, *41*, 21–31.
[131] R. E. Critoph, *Carbon* **1989**, *27*, 63–70.
[132] M. Pons, J. J. Guilleminot, *J. Sol. Energy Eng.* **1986**, *108*, 332–337.
[133] L. W. Wang, J. Y. Wu, R. Z. Wang, Y. X. Xu, S. G. Wang, X. R. Li, *Appl. Therm. Eng.* **2003**, *23*, 1605–1617.
[134] L. W. Wang, R. Z. Wang, Z. S. Lu, C. J. Chen, K. Wang, J. Y. Wu, *Carbon* **2006**, *44*, 2671–2680.
[135] L. Garzon-Tovar, J. Perez-Carvajal, I. Imaz, D. Maspoch, *Adv. Funct. Mater.* **2017**, *27*, 1606424.
[136] I. S. Girnik, A. D. Grekova, T. X. Li, R. Z. Wang, P. Dutta, S. P. S. Murthy, Y. I. Aristov, *Renewable Sustainable Energy Rev.* **2020**, *123*, 109748.
[137] T. X. Li, R. Z. Wang, T. Yan, *Energy* **2015**, *84*, 745–758.
[138] Advanced Research Projects Agency-DOE, HEATS Program Overview, https://arpa-e.energy.gov/sites/default/files/documents/files/HEATS_ProgramOverview.pdf, accessed Aug, **2020**.
[139] Y. Sun, A. Spieß, C. Jansen, A. Nuhnen, S. Gökpinar, R. Wiedey, S.-J. Ernst, C. Janiak, *J. Mater. Chem. A* **2020**, *8*, 13364.
[140] S. Graf, F. Redder, U. Bau, M. de Lange, F. Kapteijn, A. Bardow, *Energy Technol.* **2020**, *8*, 1900617.

Received: September 3, 2020